

# Storage of magnetic flux at the bottom of the solar convection zone

M. Rempel<sup>1</sup>, M. Schüssler<sup>1</sup>, and G. Tóth<sup>2</sup>

<sup>1</sup> Max-Planck-Institut für Aeronomie, Max-Planck-Strasse 2, 37191 Katlenburg-Lindau, Germany (rempe@linmpi.mpg.de; schuessler@linmpi.mpg.de)

<sup>2</sup> Loránd Eötvös University, Pázmány Péter sétány 1/A, 1117 Budapest, Hungary (gtoth@hermes.elte.hu)

Received 7 July 2000 / Accepted 26 September 2000

**Abstract.** We consider the mechanical equilibrium of a layer of axisymmetric toroidal magnetic field located in a subadiabatically stratified region near the bottom of the solar convection zone, with particular emphasis on the effects of spherical geometry. We determine equilibrium configurations and simulate numerically how these are reached from a non-equilibrium initial situation. While a subadiabatic stratification is essential for suppressing the buoyancy force, the latitudinal component of the magnetic curvature force is balanced by a latitudinal pressure gradient (in the case of a large subadiabaticity, as in the radiative interior) or by the Coriolis force due to a toroidal flow along the field lines (in the case of small subadiabaticity, as in a layer of convective overshoot). The latter case is found relevant for storing the magnetic flux generated by the solar dynamo. The corresponding equilibrium properties are similar to those of isolated magnetic flux tubes. Significant variations of the differential rotation at the bottom of the convection zone in the course of the solar cycle are expected for such a kind of equilibrium.

**Key words:** magnetic fields – Magnetohydrodynamics (MHD) – Sun: interior – Sun: magnetic fields

## 1. Introduction

Simulations of rising magnetic flux tubes in the solar convection zone indicate that essential properties of sunspot groups require the existence of a toroidal flux system with a strength of about 10 T ( $10^5$  Gauss) at the base of the convection zone (Choudhuri & Gilman 1987; D’Silva & Choudhuri 1993; Fan et al. 1993; Schüssler et al. 1994; Caligari et al. 1995, 1998).

According to the current paradigm of the dynamo process, toroidal field is generated by the rotational shear in the ‘tachocline’ (Spiegel & Zahn 1992; Charbonneau et al. 1999) near the bottom of the convection zone whereas the weaker poloidal field is produced either by cyclonic convection in the lower half of the convection zone (Parker 1993; MacGregor & Charbonneau 1997) or by the action of the Coriolis force on rising flux tubes (Leighton 1969; Wang & Sheeley 1991). The

poloidal field in the convection zone is thought to be transported to the shear layer by convective pumping (Tobias et al. 1998), turbulent diffusion or meridional circulation (Choudhuri et al. 1995; Durney 1995). The problem is to keep the toroidal flux from escaping out of the tachocline during its amplification to 10 T. In a series of papers, Parker (1987a, b, c) studies the effect of convective shielding in the context of flux storage within the superadiabatically stratified convection zone. He finds that thermal shadows can suppress the magnetic buoyancy for field strengths below 1 T. For the about 10 times stronger fields, thought to reside at the bottom of the convection zone, this effect is insufficient, so that storage requires a subadiabatic stratification as existing in a layer of convective overshoot. Consequently, there are two basic requirements for the mechanical equilibrium:

1. The temperature of the magnetized region must be lower than the unperturbed temperature of the background stratification in order to suppress the magnetic buoyancy force. The formation of such a configuration out of an initial thermal equilibrium requires a subadiabatic, convectively stable stratification so that an upward displacement leads to a rapid loss of buoyancy.
2. The latitudinal component of the magnetic curvature force has to be balanced in order to avoid a poleward slip of the whole flux system.

Moreno-Insertis et al. (1992) have considered the mechanical equilibrium of isolated magnetic flux tubes in a subadiabatic layer and the conditions under which it can be reached. They find neutrally buoyant configurations with a balance between the curvature force and the Coriolis force due to a faster rotational speed within the flux tube. However, it is not clear whether the field is in fact stored from the beginning in the form of flux tubes. A conceivable alternative is a more or less homogeneous layer of magnetic field, which generates flux tubes only after becoming unstable. Equilibria of magnetic layers have been addressed hitherto only under simplifying assumptions. Hughes (1985) and Hughes & Cattaneo (1987) consider Cartesian geometry, whereas Acheson (1979) includes curvature effects in cylindrical geometry, which is valid only in the equatorial plane of the sun. Gilman & Fox (1997) consider the influence of spherical geometry in latitude but neglect the radial dependence.

While most of these investigations focussed on the magnetic instabilities, we consider the storage of a layer of toroidal magnetic field in full spherical geometry. We first develop a perturbation model for the mechanical equilibrium of a magnetic layer (Sect. 3). We include toroidal flows and solve a system of linearized equations in the limit of large plasma beta ( $\beta = p_{\text{gas}}/p_{\text{mag}} \gg 1$ ), which is a good assumption for the deep interior of the sun. Since this approach ignores the energy equation, not all possible solutions may be physically relevant. In a second step, we therefore solve the time-dependent MHD equations in order to simulate the evolution towards a mechanical equilibrium (Sect. 4). The Versatile Advection Code<sup>1</sup> (Tóth 1996) used for these simulations has been specifically adapted to the case of low Mach numbers, which arise in our problem due to the high value of  $\beta$  and the small values of the superadiabaticity  $|\delta|$  in the deep convection zone. We investigate the processes and conditions that lead to mechanical equilibria in order to rule out solutions that cannot be reached starting from a non-equilibrium if the energy equation is included. The influence of differential rotation is considered in Sect. 5. We discuss the consequences of our results for the storage of magnetic field in the solar interior in Sect. 6 and give our conclusions in Sect. 7.

## 2. Model assumptions

The general intention of this study is to characterize the basic conditions for the storage of a strong (10 T) magnetic field near the interface between the convective zone and the underlying radiative zone and to determine the properties of the corresponding equilibrium configurations in full spherical geometry. We do not aim at modeling the formation of such a layer by the dynamical effects of differential rotation and convective flows, but concentrate on the equilibrium properties of an already strong field. Therefore, a number of simplifying assumptions is made in order to keep the problem tractable with a realistic amount of analytical and numerical effort.

We consider axisymmetric equilibrium configurations since the strong toroidal magnetic field suppresses variations in longitude owing to the curvature force. Non-axisymmetric disturbances are of interest in the case of instabilities, but in this paper we focus only on the equilibrium properties.

In the radiative interior below the convection zone the resistivity and viscosity of the plasma is sufficiently small so that we can assume ideal MHD and ignore viscosity. In the convection zone (including the overshoot layer) in principle we have to consider turbulent transport coefficients. However, the magnetic field strengths that we are dealing with are much larger than the equipartition fields with respect to the convective motions, so that we can assume these motions to be suppressed within the magnetic layer and thus ignore resistive and viscous effects as well as turbulent heat diffusion. In the convection zone outside the magnetic layer, convective energy transport and turbulent diffusion may effectively wipe out any temperature perturbation associated with the magnetic equilibrium.

It turns out, however, that such perturbations are negligible in convective and overshoot regions, so that, as far as equilibrium models are concerned, we can ignore turbulent heat transport altogether (see Sect. 4.3.5). Radiative energy transport is not suppressed by the magnetic field, but has a characteristic time scale which by far exceeds the time scales of our problem, i.e. the time to attain a mechanical equilibrium ( $\sim$  months at maximum) and the required storage time ( $\lesssim$  11 years). In fact, the radiative diffusion time  $\tau_R = \rho c_p d^2 / \kappa$  (density  $\rho = 200 \text{ kg m}^{-3}$ , specific heat  $c_p = 3.5 \cdot 10^4 \text{ J kg}^{-1} \text{ K}^{-1}$ , radiative diffusivity  $\kappa = 10^{10} \text{ W K}^{-1} \text{ m}^{-1}$ ) is of the order of 1000 years for a layer thickness of  $d = 10^4 \text{ km}$ . Likewise, the time scale for a global thermal readjustment of the Sun in response to the heat flux disturbance caused by the magnetic layer is of the order of  $10^5 \text{ yr}$ , the Kelvin-Helmholtz time of the convection zone.

Differential rotation is not considered in most of our equilibrium models. Its influence on the results is small, as estimated in Sect. 5.

## 3. Equilibrium of a magnetic layer in spherical geometry

### 3.1. Linearized equations

We consider the mechanical equilibrium of an axially symmetric toroidal field. We include a stationary toroidal flow, so that the condition for mechanical force equilibrium reads

$$\rho (\mathbf{v} \cdot \text{grad}) \mathbf{v} = -\text{grad } p + \frac{1}{\mu_0} \text{rot } \mathbf{B} \times \mathbf{B} + \rho \mathbf{g} \quad (1)$$

with the velocity  $\mathbf{v}$ , magnetic field  $\mathbf{B}$ , pressure  $p$ , density  $\rho$ , the gravitational acceleration  $\mathbf{g}$ , and the magnetic induction constant  $\mu_0 = 4\pi \cdot 10^{-7} \text{ Vs(Am)}^{-1}$ . In spherical coordinates  $(r, \theta, \phi)$  this leads to the following system of equations:

$$\frac{\partial}{\partial r} \left( p + \frac{B^2}{2\mu_0} \right) = \rho \frac{v^2 - v_A^2}{r} - \rho g, \quad (2)$$

$$\frac{\partial}{\partial \theta} \left( p + \frac{B^2}{2\mu_0} \right) = \rho (v^2 - v_A^2) \cot \theta. \quad (3)$$

Here  $v(r, \theta)$  and  $B(r, \theta)$  are the  $\phi$ -components of velocity and magnetic field,  $v_A^2 = B^2 / (\mu_0 \rho)$  is the Alfvén speed and  $g = |\mathbf{g}|$ . For all conceivable values of the field strength in the deep convection zone we have  $\beta \equiv p_{\text{gas}}/p_{\text{mag}} \gg 1$ , so that the magnetic field causes only a slight perturbation of the background stratification. In this case we can decompose pressure and density into values for their background stratification ( $p_0, \rho_0$ ) and a small perturbation caused by the magnetic field ( $p_1, \rho_1$ ). After subtraction of the hydrostatic background (including the effect of a rigid rotation with the velocity  $v_0 = \Omega_0 r \sin \theta$ ) and a linearization we obtain for slow rotation ( $v_0^2 \ll g r$ ):

$$\frac{\partial}{\partial r} \left( p_1 + \frac{B^2}{2\mu_0} \right) = \rho_0 \frac{v^2 - v_0^2 - v_A^2}{r} - \rho_1 g, \quad (4)$$

$$\frac{\partial}{\partial \theta} \left( p_1 + \frac{B^2}{2\mu_0} \right) = \rho_0 (v^2 - v_0^2 - v_A^2) \cot \theta. \quad (5)$$

By differentiating Eq. (4) with respect to  $\theta$  and Eq. (5) with respect to  $r$ , this system of partial differential equations can be

<sup>1</sup> <http://www.phys.uu.nl/~toth>

reduced to a decoupled pair of ordinary differential equations in  $\theta$ -direction:

$$\frac{\partial p_1}{\partial \theta} = \left[ \varrho_0 (v^2 - v_0^2) - \frac{B^2}{\mu_0} \right] \cot \theta - \frac{\partial}{\partial \theta} \left( \frac{B^2}{2\mu_0} \right), \quad (6)$$

$$\frac{\partial \varrho_1}{\partial \theta} = \frac{1}{g r} \frac{\partial}{\partial \theta} \left[ \varrho_0 (v^2 - v_0^2) - \frac{B^2}{\mu_0} \right] - \frac{\cot \theta}{g} \frac{\partial}{\partial r} \left[ \varrho_0 (v^2 - v_0^2) - \frac{B^2}{\mu_0} \right]. \quad (7)$$

This pair of equations can be integrated after specifying  $v(r, \theta)$  and the radial profile of the pressure perturbation  $p_1(r, \theta_0)$  for a chosen colatitude  $\theta_0$ . The corresponding density profile  $\varrho_1(r, \theta_0)$  follows from Eq. (4). For a given magnetic field  $B(r, \theta)$  we have the following degrees of freedom for the equilibrium solution:

- choice of a toroidal flow  $v(r, \theta)$  (e.g. a given differential rotation),
- choice of the profile  $p_1(r, \theta_0)$ .

Not all of these possible equilibria are physically relevant, since for a consistent solution we have to consider the energy equation as well. In Sect. 4 we solve the time dependent MHD-equations including the energy equation in order to simulate the evolution towards an equilibrium.

### 3.2. Solutions

We solve Eqs. (6) and (7) for a magnetic field at the bottom of the convection zone. For the background stratification we use a polytropic atmosphere with  $g \sim r^{-2}$ . The values of pressure, density, and gravitational acceleration at  $r_0 = 5 \cdot 10^8$  m are  $p_0 = 6 \cdot 10^{12}$  Pa,  $\varrho_0 = 200$  kg m $^{-3}$ , and  $g_0 = 500$  m s $^{-2}$ . The possible solutions of Eqs. (6) and (7) can be divided into two types:

- solutions with a dominant role of a toroidal flow,
- solutions with a dominant role of a pressure gradient in  $\theta$ -direction.

The simplest solution of the first type is characterized by the following conditions:

$$\varrho_1 = 0, \quad (8)$$

$$p_1 = -\frac{B^2}{2\mu_0}, \quad (9)$$

$$v = \sqrt{v_0^2 + v_A^2}. \quad (10)$$

Note that this solution is similar to the equilibrium of a flux tube in the overshoot region as discussed by Moreno-Insertis et al. (1992): the magnetic curvature force is balanced by the Coriolis force due to the toroidal flow. Neutral buoyancy (Eq. (8)) and pressure balance (Eq. (9)) lead to a lower temperature within the magnetic layer; the temperature perturbation is about 10 K for a field strength of 10 T. The basic solution can be generalized by adding a solution  $(\tilde{\varrho}_1, \tilde{p}_1)$  that fulfills

$$\frac{\partial \tilde{p}_1}{\partial r} = -\tilde{\varrho}_1 g, \quad (11)$$

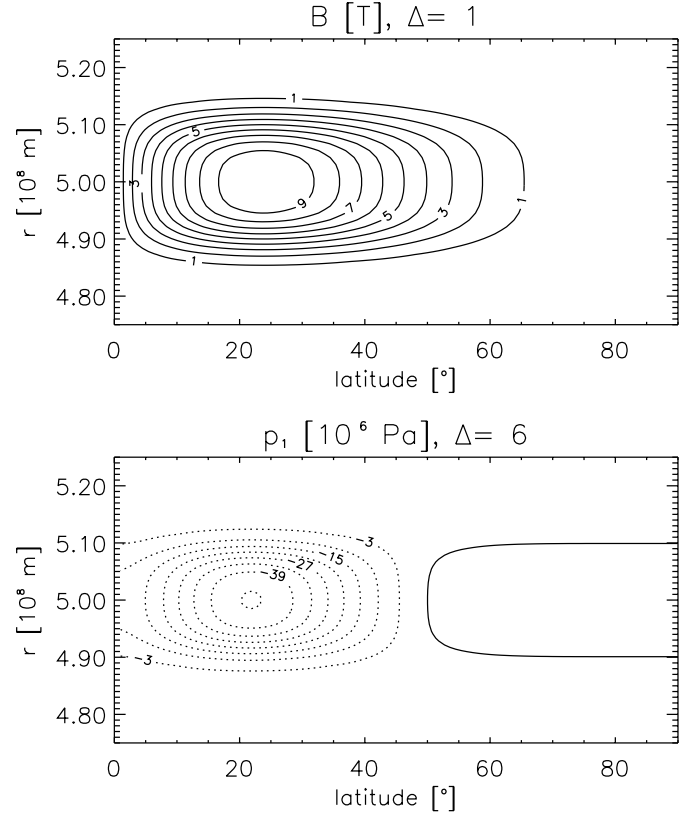


**Fig. 1.** Isolines of the magnetic field strength ( $B$ ) and the perturbation of the gas pressure ( $p_1$ ) for a magnetic layer without toroidal flow. The figures show a segment of the  $r - \theta$  plane, which is represented in a rectangular fashion for better visibility (latitude =  $90^\circ - \theta$ ). The symbol  $\Delta$  denotes the distance of the contour levels in the units given within the angular brackets.

$$\frac{\partial \tilde{p}_1}{\partial \theta} = \frac{\partial \tilde{\varrho}_1}{\partial \theta} = 0.$$

The numerical results presented in Sect. 4 show a solution corresponding to this generalized type. The additional changes of pressure, density and temperature are smaller than  $\mathcal{O}(1/\beta)$ .

The perturbation of the rotational speed by the toroidal flow  $v(r, \theta)$  can be estimated as:

$$v - v_0 \approx \frac{1}{2} \frac{B^2}{\mu_0 \varrho \Omega_0 r \sin \theta} \sim 2 \left( \frac{B}{1 \text{ T}} \right)^2 \text{ m s}^{-1} \quad (12)$$

( $\Omega_0 = 2.6 \cdot 10^{-6}$  s $^{-1}$ ,  $r = 5 \cdot 10^8$  m,  $\varrho = 200$  kg/m $^3$  and  $\theta = 45^\circ$ ). Consequently, for a field of the order of 10 T, the perturbation of the rotational flow required for the equilibrium is comparable to the velocity difference due to differential rotation as inferred from helioseismology (e.g. Charbonneau et al. 1999).

The second type of solution is obtained by setting  $v = v_0$ . As an example, we take a magnetic field with a maximum field strength of 10 T at  $\theta = 65^\circ$  ( $25^\circ$  latitude) and choose the initial condition as  $p_1 = -B^2/(2\mu_0)$  for  $\theta = 60^\circ$ . Such a profile is the typical result of the numerical simulations (cf. Sect. 4). Figs. 1 and 2 show the field strength distribution and the corresponding perturbations of pressure and density for the equilibrium configuration.

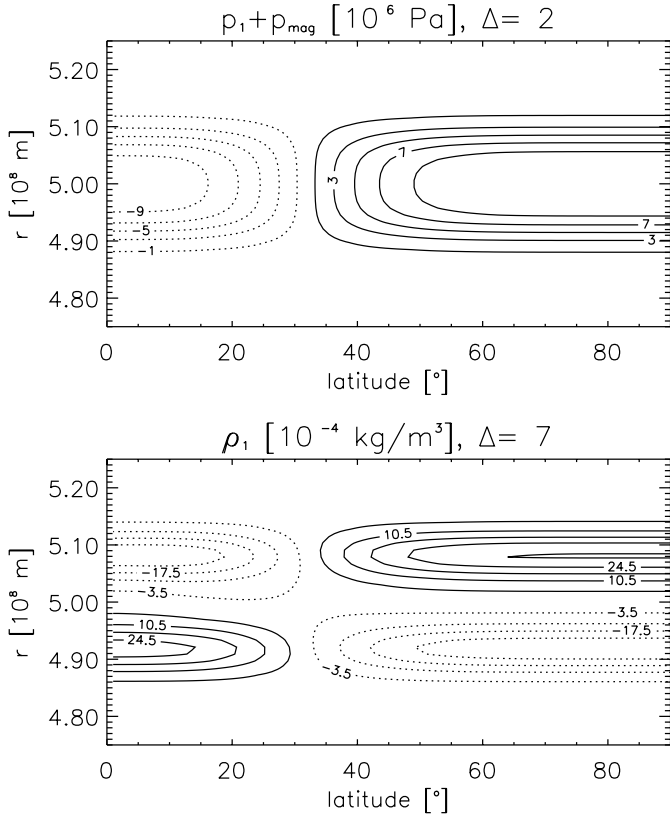


**Fig. 2.** Isolines of the total pressure perturbation ( $p_1 + p_{\text{mag}}$ ) and the density perturbation ( $\varrho_1$ ) for the same case as shown in Fig. 1. The magnetic curvature force is compensated by the latitudinal gradient of the total pressure perturbation. The hydrostatic equilibrium in the radial direction requires a density perturbation proportional to the radial gradient of the total pressure perturbation.

In contrast to the first case, for which the perturbation of the density vanishes (or is given by the generalized solution with a relative magnitude less than  $1/\beta$ ), the second case requires a non-negligible density perturbation, which is mainly dependent on the gradient of the magnetic field. We estimate roughly the magnitude of this perturbation, ignoring factors  $\propto \cot \theta$  which are of  $\mathcal{O}(1)$ . The perturbation of the pressure consists of two contributions: 1) the perturbation due to the magnetic pressure and 2) the pressure profile that is necessary to compensate the curvature force (cf. Fig. 2, upper panel). Both contributions are of  $\mathcal{O}(1/\beta)$ . The corresponding density perturbation follows from Eq. (4):

$$\frac{\varrho_1}{\varrho_0} \sim \frac{1}{\beta} \frac{p_0}{\varrho_0 g d} \sim \frac{1}{\beta} \frac{H_p}{d}, \quad (13)$$

where  $d$  is the thickness of the magnetic layer and  $H_p$  the pressure scale height ( $\approx 6 \cdot 10^7$  m). Since  $d \ll H_p$  at the bottom of the convection zone, the relative density perturbation is much larger than the relative pressure perturbation. From the linearized ideal gas equation,

$$\frac{T_1}{T_0} = \frac{p_1}{p_0} - \frac{\varrho_1}{\varrho_0}, \quad (14)$$

it follows that the relative temperature perturbation is basically equal to the negative relative density perturbation.

The general properties of the equilibria are not strongly dependent upon the assumed distribution of the magnetic field in latitude. The background stratification has no significant influence on the equilibria since the variation of the background values (on a scale of  $H_p$ ) is small within the layer (as long as  $d \ll H_p$ ). A more important effect of the background stratification is due to the value of the superadiabaticity,  $\delta = \nabla - \nabla_{\text{ad}}$ , which affects the energy equation as discussed in detail in the following section.

## 4. MHD-simulations

### 4.1. Setup

The equilibrium configurations for magnetic layers discussed above are of practical interest only if they can be reached from a non-equilibrium state. In order to study this process, its time scale, and the dependence on the superadiabaticity  $\delta = \nabla - \nabla_{\text{ad}}$  of the background stratification, we have performed numerical simulations of the axisymmetric time-dependent MHD equations using the Versatile Advection Code.

To serve our purposes we have introduced a number of modifications to the code:

- Since the original code has no spherical polar coordinates, we use cylindrical polar coordinates and add geometrical source terms while maintaining mass conservation.
- In order to deal with the small Mach numbers resulting from the large values of  $\beta$ , we have used the MacCormack scheme, which introduces a very small numerical viscosity, and have rewritten the MHD equations in terms of perturbations with respect to the (hydrostatic) background stratification.
- The small value of  $|\delta|$  in the overshoot region and lower convection zone leads to problems of numerical accuracy that can be avoided by rewriting the energy equation in terms of the specific entropy. Decomposing the entropy into the value of the background stratification and an entropy perturbation allows us to use directly the superadiabaticity  $\delta$  of the background stratification without having to take numerical derivatives, whose error would be comparable to the value of the small superadiabaticity itself.

The entropy per unit mass

$$s = c_v \ln \left( \frac{p}{\varrho^\gamma} \right) \quad (15)$$

( $c_v$ : specific heat at constant volume) satisfies the equation

$$\frac{ds}{dt} = \frac{\partial s}{\partial t} + \mathbf{v} \cdot \text{grad } s = 0, \quad (16)$$

where  $\mathbf{v}$  is the meridional velocity. Decomposing the entropy into the time-independent value of the background stratification ( $s_0$ ) and an entropy perturbation ( $s_1$ ) leads to:

$$\frac{\partial s_1}{\partial t} + \mathbf{v} \cdot \text{grad } s_1 = -\mathbf{v} \cdot \text{grad } s_0. \quad (17)$$

Since the influence of the centrifugal force on the background stratification can be neglected for solar rotation, the gradient of  $s_0$  has only a non-vanishing radial component, which can be expressed in terms of the superadiabaticity  $\delta$ :

$$\frac{ds_0}{dr} = -\frac{c_p \delta}{H_p} \quad (18)$$

( $c_p$ : specific heat at constant pressure). Transforming the entropy equation into a conservation form leads to

$$\frac{\partial}{\partial t} (\varrho s_1) + \operatorname{div}(\mathbf{v} \varrho s_1) = \varrho v_r \frac{c_p \delta}{H_p}. \quad (19)$$

In this way, we have separated the effects caused by a non-adiabatic background stratification (term on the right hand side), into which the quantity  $\delta$  enters explicitly. Eq. (19) can easily be generalized to include thermal diffusion or other processes by adding the corresponding terms to the right hand side.

#### 4.2. Grid, boundary conditions, and initial state

The calculations are performed in a hemispherical shell extending in latitude from pole to equator. The grid size typically used is 80 grid points in radial direction and 40 grid points in latitudinal direction. In order to resolve the magnetic layer sufficiently, we use a non-uniform grid in radial direction with smaller grid cells within the layer. The required minimum grid spacing depends on the thickness of the layer, the gradients of the magnetic field and the background stratification (e.g. if there is a sharp transition between radiation zone and overshoot region).

All boundaries are closed and free-slip conditions are assumed (mass flux perpendicular to the boundary antisymmetric, parallel to the boundary symmetric). This corresponds to our assumptions of axial symmetry as well as symmetry with respect to the equatorial plane, but may seem somewhat arbitrary at the top and bottom boundaries. However, the lower boundary is placed in the radiative interior where the strong subadiabatic stratification effectively suppresses radial motions. The upper boundary can be moved sufficiently outward, so that its influence on the solution is minimized.

We consider three different configurations for the initial state:

- *Temperature equilibrium (TEQ)*: The temperature in the magnetic layer is equal to the temperature of the background stratification.
- *Radial force equilibrium (REQ)*: The temperature in the magnetic layer is chosen in such a way that the buoyancy force compensates the radial component of the curvature force.
- *Latitudinal force equilibrium (LEQ)*: The temperature is chosen as in TEQ. The magnetic curvature force is compensated by the Coriolis force due to a toroidal flow.

By considering REQ and LEQ we can study separately the processes that lead to an equilibrium in radial and latitudinal direction, respectively, while TEQ lets them operate simultaneously. In all initial states the magnetic pressure is balanced by the gas

pressure perturbation since this equilibrium is established most rapidly.

These initial conditions are somewhat artificial since we start with a strong magnetic field that is not in mechanical equilibrium. In reality, such a strong field would be amplified over a longer time scale and would evolve in a quasi-stationary manner while always maintaining approximate mechanical equilibrium. We choose these conditions nevertheless in order to study the basic physical processes leading to an equilibrium and determining its properties. In order to reach the stationary equilibrium, we have included a simple damping term proportional to the meridional velocities.

### 4.3. Results

#### 4.3.1. An illustrative example

We first illustrate the importance of storing strong magnetic field in an equilibrium configuration. To this end, we simulate the evolution of a magnetic layer at the bottom of an adiabatically stratified convection zone, ignoring rotation. We assume initial force balance in the radial direction, whereas the latitudinal component of the magnetic curvature force is not balanced. The result is shown in Fig. 3: within less than a month, the curvature force leads to a drastic drift towards the pole. The flow field driven by the curvature force is a circulation flow, which is poleward at the bottom and equatorward at the top of the convection zone. The corresponding radial upflow is located between  $40 - 60^\circ$  and leads to a radial transport of magnetic flux in the convection zone. This shows clearly that mechanical equilibrium in spherical geometry requires latitudinal force balance, compensation of the buoyancy force is not sufficient.

#### 4.3.2. General remarks

The results presented in the following subsections are calculated for a rigid background rotation. The additional effects caused by a solar-like differential rotation are considered in Sect. 5.

If we start from a temperature equilibrium (TEQ), the buoyancy force leads to an upward drift of the magnetic layer, whereas the latitudinal component of the curvature force drives a flow towards the pole. We separately discuss the processes which lead to force balance in radial and latitudinal direction, since these processes are of different physical nature and involve different time scales.

#### 4.3.3. Establishment of the latitudinal force balance

If we start from REQ, the unbalanced curvature force leads to the characteristic flow pattern shown in Fig. 4. The curvature force drives a two-cell flow with poleward motion within the layer. Since the subadiabatic stratification suppresses radial motions, the equatorward return flow is localized in two bands above and below the layer. The corresponding radial flow pattern shows up- and downflows at the equator and at about  $50^\circ$  latitude. The combination of two processes is crucial here:

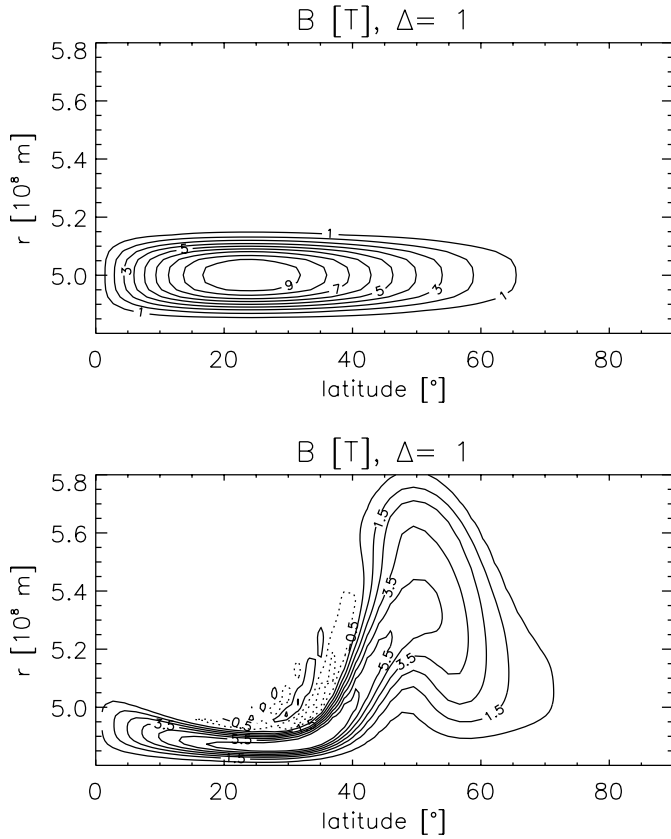


**Fig. 3.** Drift of a magnetic layer driven by an unbalanced magnetic curvature force in the absence of rotation. Upper panel: isolines of  $B$  for the initial state (same as in Fig. 1), lower panel: after 1 month simulated time. The simulation is performed with an adiabatic background stratification ( $\delta = 0$ ) and starting with force balance in radial direction.

firstly, the transport of angular momentum by the meridional motion leads to a toroidal flow (relative to the background rotation), which tends to balance the curvature force by means of the Coriolis force (with a time scale comparable to the rotation period); secondly, the radial motions in a subadiabatic stratification generate temperature perturbations relative to the ambient stratification (the plasma is cooler in an upflow and warmer in a downflow), building up a latitudinal pressure gradient (with time scale  $\propto |\delta|^{-1/2}$ , cf. Eq. (24)). These two processes tend to establish the two types of equilibrium configurations discussed in Sect. 3. In the first case, the magnetic curvature force is compensated by the Coriolis force; only a small perturbation of the stratification is required to balance the perturbation of the total pressure gradient. In contrast, the second process leads to larger perturbations of the stratification (cf. Figs. 1, 2). The magnitude of the superadiabaticity of the background stratification determines which of the two processes dominates:

- $\delta_0 \approx -0.1$  (radiation zone): Mechanical equilibrium is established in  $\approx 10^5$  s; the influence of a toroidal flow can be neglected in comparison to that of the latitudinal pressure gradient;
- $\delta_0 \approx -10^{-3}$  (overshoot region): Mechanical equilibrium is established in  $\approx 10^6$  s; both effects are comparable;

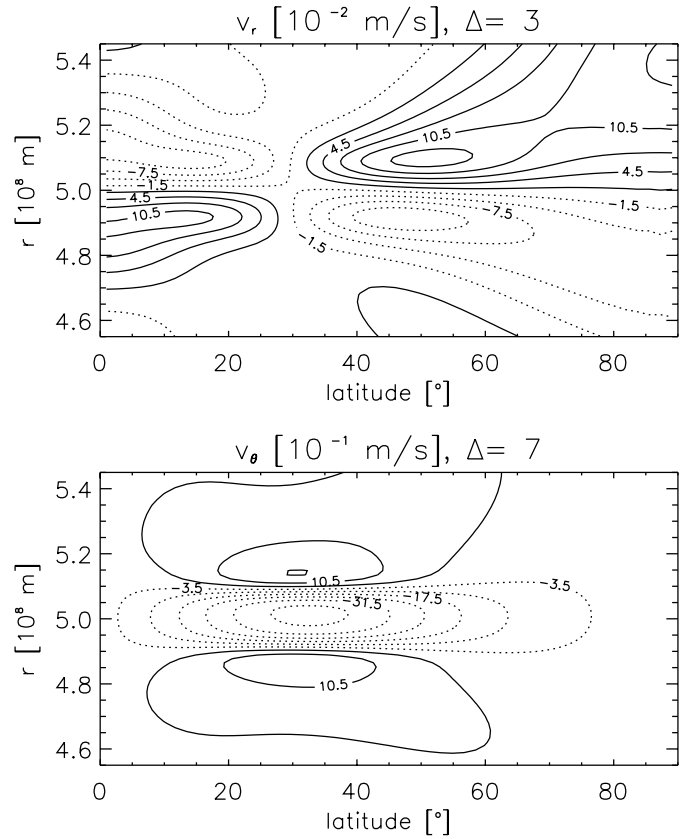


**Fig. 4.** Isolines of the meridional velocity field after  $2 \cdot 10^4$  s simulated time, starting from the magnetic field shown in Fig. 1 and assuming initial force balance in the radial direction. The superadiabaticity of the background stratification is  $\delta = -0.1$ , corresponding to the radiation zone. The curvature force drives a two-cell flow. The lower panel shows the latitudinal velocity, which is poleward directed within the layer (dotted lines). The corresponding radial flow is shown in the upper panel. Here solid lines correspond to upflows.

- $\delta_0 > -10^{-3}$  (overshoot region and convection zone): The equilibrium is determined by the toroidal flow.

The time scale  $\tau$  for the establishment of the equilibrium and its dependence on the superadiabaticity of the background stratification can roughly be estimated as follows.

*Strongly subadiabatic stratification (radiation zone):*

A mechanical equilibrium requires temperature fluctuations of the order of (see Eqs. (13) and (14)):

$$\frac{T_1}{T_0} \sim \frac{H_p}{d} \frac{B^2}{2\mu_0 p}. \quad (20)$$

Radial motions in a subadiabatic stratification lead to temperature perturbations with a magnitude of (Eq. (19)) together with  $s_1 \approx c_p T_1/T_0$

$$\frac{T_1}{T_0} \sim |\delta| \frac{v_r \tau}{H_p}. \quad (21)$$

For the mean velocity of the poleward directed flow, the momentum equation yields (linear regime)

$$v_\theta \sim \frac{1}{2} \frac{B^2}{\mu_0 \varrho r} \tau, \quad (22)$$

which determines  $v_r$  by means of the continuity equation:

$$v_r \sim v_\theta \frac{d}{\pi/2r}. \quad (23)$$

Solving for  $\tau$  yields, ignoring numerical factors of order unity:

$$\tau \sim \sqrt{\frac{H_p^2 r^2 \varrho}{p d^2 |\delta|}}. \quad (24)$$

With  $H_p = 6 \cdot 10^7$  m,  $r = 5 \cdot 10^8$  m,  $\varrho = 200$  kg m<sup>-3</sup>,  $p = 6 \cdot 10^{12}$  Pa,  $\delta = -0.1$  and  $d \sim 10^7$  m we obtain  $\tau \sim 5 \cdot 10^4$  s, which is in a good agreement with the results of the numerical simulation.

*Weakly subadiabatic stratification (overshoot layer):*

The latitudinal displacement due to the magnetically driven flow can be estimated as

$$r \Delta\theta \sim v_\theta \tau \sim \frac{B^2}{2\mu_0 \varrho r} \tau^2. \quad (25)$$

Angular momentum conservation gives

$$v_{\phi 0} r_0 \sin \theta_0 = (v_{\phi 0} + v_{\phi 1}) r_0 \sin(\theta_0 + \Delta\theta), \quad (26)$$

so that we find for the perturbation of the toroidal velocity ( $\cot \theta_0 \approx 1$ ):

$$v_{\phi 1} \sim v_{\phi 0} \Delta\theta \sim v_{\phi 0} \frac{B^2}{2\mu_0 \varrho r^2} \tau^2. \quad (27)$$

The force equilibrium between Coriolis force and magnetic curvature force requires

$$B^2 \sim 2\mu_0 \varrho v_{\phi 0} v_{\phi 1} \sim v_{\phi 0}^2 \frac{B^2}{r^2} \tau^2. \quad (28)$$

Ignoring numerical factors of order unity, we find

$$\tau \sim \frac{v_{\phi 0}}{r} \sim \frac{1}{\Omega}. \quad (29)$$

The two time scales in Eqs. (24) and (29) become comparable for

$$|\delta| \sim \frac{H_p^2 r^2 \varrho}{p d^2} \Omega^2. \quad (30)$$

Inserting the values given above and using the solar rotation rate we find from Eq. (30) a value of  $|\delta| \sim 10^{-3}$ , which is in good agreement with the results from the simulations. If we have strong viscous damping, the evolution towards an equilibrium takes longer, but the critical superadiabaticity, for which both processes have the same magnitude, is not strongly affected. Note that in both cases the time scales are independent of the field strength.

The evolution towards an equilibrium is not strongly dependent on the initial location of the magnetic field. The influence of the  $\cot \theta$  dependence, which we have neglected in the discussion above, leads to somewhat longer time scales near to the equator.

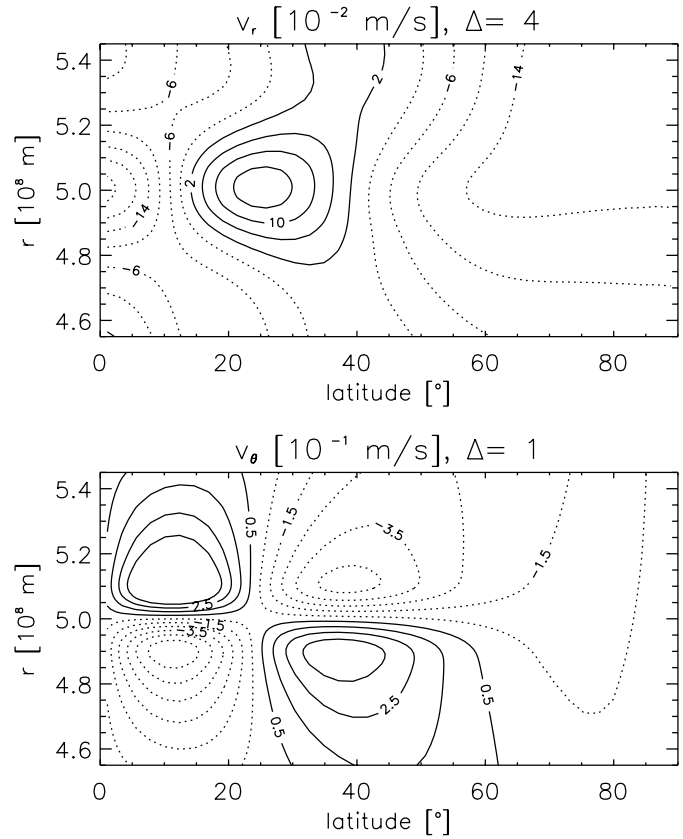


**Fig. 5.** Isolines of the meridional velocity field after  $5 \cdot 10^3$  s starting with the same magnetic field as in Fig. 4, but assuming initial force balance in the latitudinal direction. The unbalanced buoyancy force leads to an upflow in the region of strongest magnetic field around  $25^\circ$  latitude, whereas a downflow develops in the weak-field region near to the equator and the pole.

#### 4.3.4. Establishment of radial force balance

In the case of isolated magnetic flux tubes, the compensation of the buoyancy force can be described as follows (cf. Moreno-Inertis et al. 1992): As a buoyant flux tube rises in a subadiabatic stratification, it becomes cooler than the external plasma. The corresponding loss of buoyancy leads to an oscillation around the equilibrium position. The time scale for this process is roughly given by the Brunt-Väisälä frequency:

$$\tau_{BV} \sim \sqrt{\frac{H_p}{|\delta|g}}. \quad (31)$$

The equilibrium state is a flux tube with the same density as the surrounding plasma. For a magnetic layer, the situation is somewhat different because the flow driven by buoyancy also affects the non-magnetized plasma. Fig. 5 gives an example of the flow pattern arising from an initial state with a net buoyancy force. The magnetic field is the same as in Fig. 1. The buoyancy force drives an upflow located around the peak field at  $25^\circ$  latitude. Downflows develop in the regions with weak field near the equator and above  $45^\circ$  latitude. Due to the subadiabatic stratification, the plasma is cooler in the upflow and warmer in the downflow

region. The temperature profile of the equilibrium state finally reached in the simulation is shown in Fig. 6. The corresponding density perturbation is nearly independent of latitude. The temperature perturbation is such that the magnetic buoyancy in the region of strong field and the thermal buoyancy in the region of weak field have the same size; both are compensated by a radial pressure gradient. This is in contrast to the equilibrium of flux tubes with neutral buoyancy. The time required to establish this kind of equilibrium is about  $100 \tau_{BV}$ . However, the initial buoyant upflow is already suppressed after  $5 - 10 \tau_{BV}$ . Inserting  $H_p = 6 \cdot 10^7$  m and  $g = 500 \text{ m s}^{-2}$  in Eq. (31) leads to  $\tau_{BV} \sim 10^3$  s for  $\delta = -0.1$  (radiation zone) and  $\tau_{BV} \sim 10^5$  s for  $\delta = -10^{-5}$  (overshoot region). This means that the time scale for compensating the buoyancy is smaller than the time scale needed to suppress the poleward drift in the radiation zone, whereas both become comparable in the overshoot region.

The radial distance that is covered during the period of upward motion can be roughly estimated from Eq. (21) as

$$\Delta r \sim \frac{H_p}{\beta|\delta|}. \quad (32)$$

In the radiation zone  $\Delta r$  is of the order of a few kilometers. In the case of storage in the overshoot region  $\Delta r$  should be less than the thickness of the overshoot region. Taking  $\Delta r \lesssim 10^7$  m,  $\delta \lesssim -4 \cdot 10^{-5}$  is required for the storage of a field of 10 T. This is in good agreement with the estimates of Moreno-Insertis et al. (1992) for the case of flux tubes.

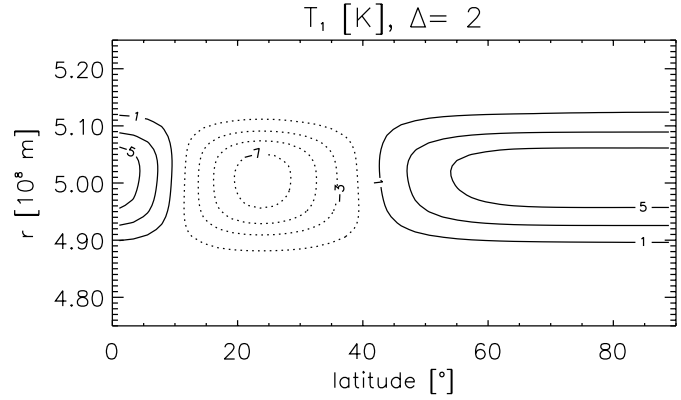
#### 4.3.5. Simulation starting from TEQ

Fig. 7 shows three snapshots of the evolution towards an equilibrium starting from TEQ. We use a solar-like background stratification with the transition between the radiative core ( $\delta \approx -0.2$ ) and the overshoot region ( $\delta \approx -5 \cdot 10^{-5}$ ) at  $r = 10^8$  m. Since the magnetic field straddles the interface between both regions, we simultaneously obtain the two types of evolution. The processes discussed separately in Sect. 4.3.3 and 4.3.4 become visible in the order of their respective time scale.

The shortest time scale corresponds to the suppression of buoyancy in the radiation zone. The resulting temperature perturbation shown in the top panel of Fig. 7 is comparable to the pattern shown in Fig. 6. The mid panel shows mainly the establishment of the latitudinal pressure gradient in the radiation zone. The influence of the toroidal flow of a few  $\text{m s}^{-1}$  can be neglected for the force balance. The generation of the strong toroidal flow in the overshoot region takes about 10 times longer and requires a poleward drift of  $5 \dots 10^\circ$  as can be seen in the bottom panel, while the drift of the magnetic field can be neglected in the radiative zone.

The bottom sequence shows a state near to the final equilibrium. The remaining latitudinal velocities are about  $1 \text{ m s}^{-1}$  compared to a maximum speed during the evolution of about  $60 \text{ m s}^{-1}$ .

This sequence shows clearly the difference between the equilibria in the radiation zone and the those in the overshoot region. Whereas temperature fluctuations of about 60 K are re-



**Fig. 6.** Isolines of the temperature perturbation for an equilibrium state resulting from initial force imbalance in radial direction. The buoyancy of the initial state drives an upflow in the region with the highest field strength, the corresponding downflows are localized in the regions of weak magnetic field. The resulting temperature perturbation due to the subadiabatic stratification shows a lower temperature in the region of strong field strength and a higher temperature in the region of low field strength.

quired in the radiation zone, the fluctuations within the overshoot region are smaller by a factor 10 or more. Since these fluctuations are not significant for the equilibrium in latitudinal direction, including turbulent thermal diffusion outside the magnetic field would not affect the equilibrium. The temperature profile leading to radial force balance shown in Fig. 6 may be affected near pole and equator, but this would only result in a slight upward displacement until the state of neutral buoyancy is achieved (similar to flux tubes). In this case, the temperature fluctuations are present only in the magnetized region, where the convection is suppressed. A similar argument applies to the effect of viscosity on the toroidal flow. The strong toroidal flow that balances the magnetic tension is located within the magnetic field, where turbulent motions are suppressed. If the toroidal flow outside the layer would be wiped out by adding a turbulent viscosity, this would not be relevant for the equilibrium. This justifies a posteriori our assumptions concerning the turbulent transport coefficients in Sect. 2.

## 5. Effect of differential rotation

In the results presented so far, we have neglected the influence of differential rotation, namely

- 1) Differential rotation changes the angular momentum distribution.
- 2) Differential rotation leads to a Coriolis force in the uniformly rotating frame of reference defined by the rigid rotation of the core.

The first point affects the angular momentum transport, which is important for the establishment of equilibria with toroidal flows. This leads only to a slight change in the time scale ( $\tau \sim 1/\Omega$ ), but has no influence on the final equilibrium.

The second point has a different influence in the radiation zone and the convection zone: in the radiation zone, the Coriolis

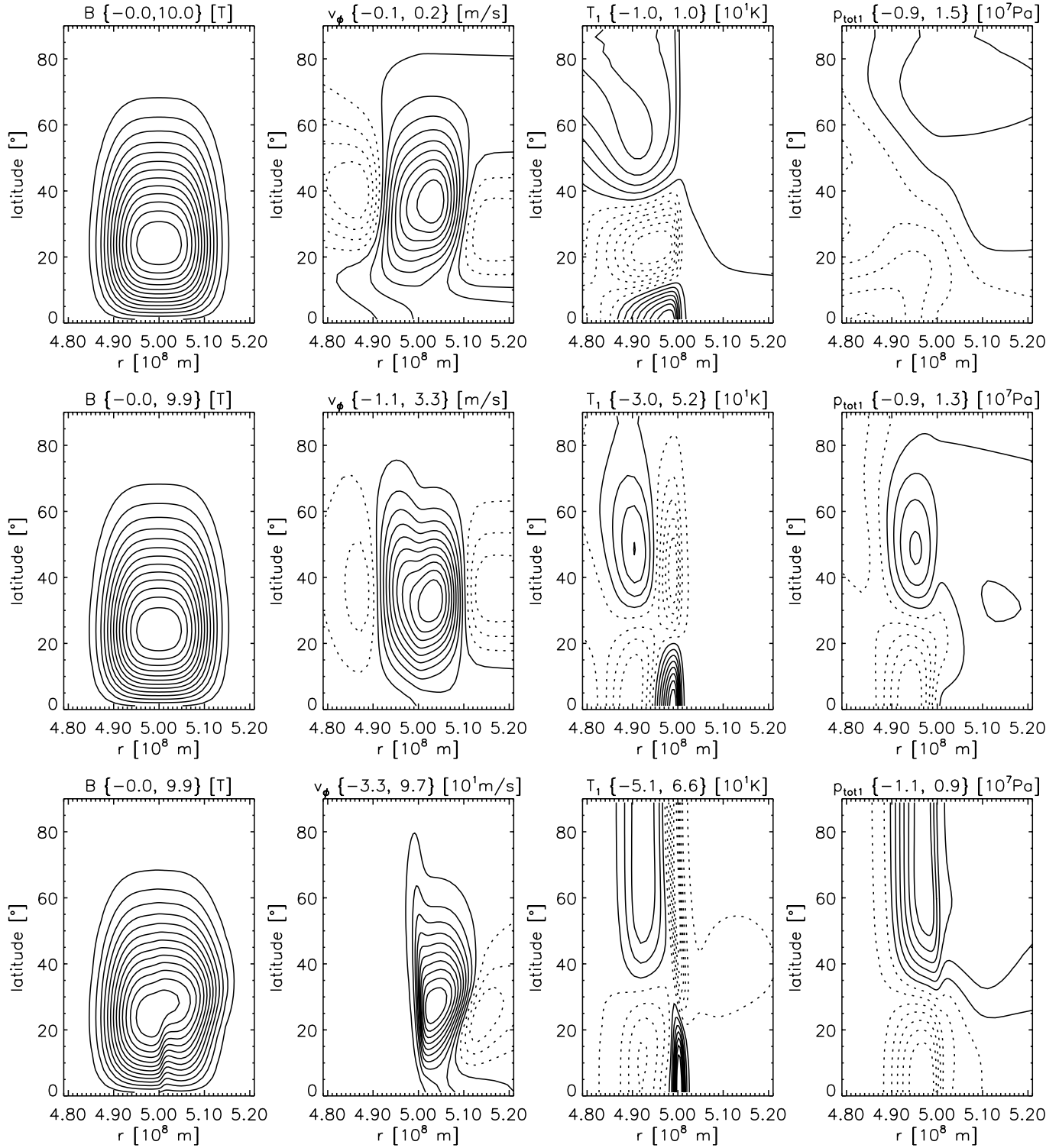


**Fig. 7.** Evolution towards an equilibrium for a magnetic layer straddling the interface between the convective zone (overshoot region,  $\delta = -5 \cdot 10^{-5}$ ) and the radiation zone ( $\delta = -0.2$ ) at  $r = 5 \cdot 10^8$  m. Shown is a time sequence (top to bottom after  $2 \cdot 10^4$  s,  $10^5$  s, and  $3 \cdot 10^6$  s, respectively) of isolines of magnetic field ( $B$ ), toroidal flow speed relative to the background rotation ( $v_\phi$ ), temperature perturbation ( $T_1$ ) and the total (magnetic+gas) pressure perturbation ( $p_{\text{tot1}}$ ). Note that these figures are rotated by  $90^\circ$  compared to the figures shown before. The minimum and maximum values of each plot are given in braces. The initial condition is temperature equilibrium (TEQ). The sequence shows first the compensation of buoyancy in the radiation zone (temperature perturbation, top panel), and then the establishment of the latitudinal equilibrium (mid and bottom panel). The about 10 times longer time scale to establish the latitudinal force equilibrium in the overshoot region (Coriolis force) compared to the corresponding time scale in the radiation zone (pressure gradient) explains the drift of the magnetic field of about  $5 - 10^\circ$  in the overshoot region.

force caused by the differential rotation is compensated by slight perturbations of the stratification (about 10 K in the temperature profile), whereas in the nearly adiabatic convection zone such an equilibrium cannot exist (Taylor-Proudman-theorem) and a meridional circulation is driven (see e.g. Rüdiger et al. 1998 for a recent model).

As a result, the pressure-balanced equilibria of a toroidal magnetic field in the radiation zone are not significantly influenced by the differential rotation. The background stratification enters the evolution towards the equilibrium mainly in terms of the superadiabaticity, which is not strongly changed by the additional perturbations due to the differential rotation.

Coriolis-force balanced equilibria in the overshoot region can be affected by the meridional circulation that is equatorward at the bottom of the convection zone. In the case of a weak field (equipartition field strength) this leads to an equatorward transport of flux. In the case of a strong magnetic field the turbulent viscosity is suppressed by magnetic field and thus the angular-momentum conservation acts against any drift of the magnetic field out of the equilibrium position. The effect on such equilibria is therefore small.

## 6. Flux storage in the solar interior

Storage of a super-equipartition field of 10 T for times comparable to a solar cycle period requires a state of mechanical equilibrium since the stresses exerted by the convective motions cannot compensate the magnetic stress. Our results show that a magnetic layer located in a weakly subadiabatic overshoot layer attains an equilibrium dominated by the Coriolis force due to a toroidal flow (superposed upon rotation). Such an equilibrium is rather similar to the equilibrium of isolated flux tubes (Moreno-Insertis et al. 1992). Flux tubes forming through a Rayleigh-Taylor-type instability of a magnetic layer would therefore find themselves already near their equilibrium configuration. The situation would be significantly different for a magnetic layer stored in the radiation zone below the convection zone. In this case, an equilibrium dominated by a latitudinal pressure gradient very much different from the equilibrium of flux tubes evolves. Flux tubes formed out of such a configuration would be far apart from their equilibrium and would start to drift poleward in order to establish the necessary toroidal flow. This may lead to problems for understanding the concentration of flux emergence in low heliolatitudes. Furthermore, the large subadiabaticity of the radiation zone stabilizes the layer so that flux tube formation requires field strength far in excess of 10 T, which would not be in agreement with many observational properties of bipolar magnetic regions on the solar surface, not to speak about the difficulties of generating such strong fields in the first place and explaining the field reversals.

We conclude that the magnetic flux responsible for solar activity is stored in a weakly subadiabatic region (e.g. an overshoot layer) in an equilibrium dominated by the Coriolis force due to toroidal flows, independent of its configuration in a layer or in the form of flux tubes. This leads to the prediction of significant temporal changes of the differential rotation in the storage re-

gion since the strength of the toroidal flux system varies strongly in the course of the solar cycle. Indeed, variations of the internal solar rotation near the bottom of the convection zone have been reported recently by Howe et al. (2000).

## 7. Conclusions

Our study of the mechanical equilibrium of magnetic layers in spherical geometry has led us to the following conclusions relevant for the storage of a strong (10 T) toroidal magnetic field near the bottom of the solar convection zone:

- Compensation of the buoyancy force requires subadiabaticity ( $\delta = \nabla - \nabla_{\text{ad}} < 0$ ) of the background stratification.
- The latitudinal component of the magnetic curvature force can be balanced either by the Coriolis force due to a toroidal flow along the field lines (Coriolis balance) or by a latitudinal pressure gradient (pressure balance) with associated temperature perturbations.
- Coriolis balance is established for magnetic layers in weakly subadiabatic regions ( $|\delta| < 10^{-3}$ ), like a layer of convective overshoot. The time scale for the evolution of the equilibrium is of the order of the rotation period. Such equilibria resemble the mechanical equilibrium of isolated flux tubes.
- Pressure balance evolves in strongly subadiabatic regions ( $|\delta| > 10^{-3}$ ), particularly in the radiative zone. The associated time scale is about one day for  $\delta = -0.1$ . For  $|\delta| \simeq 10^{-3}$  a mixture of both equilibria develops.
- Storage of a 10 T field in the convective overshoot region of the sun takes place in Coriolis balance, independent of a flux tube or layer structure of magnetic field. We expect a strong effect of the magnetic field on the differential rotation in the tachocline and thus a significant variation of the latter over the solar cycle.

*Acknowledgements.* This work has been funded by the Deutsche Forschungsgemeinschaft under grant Schu 500-8. G. Tóth is supported by a postdoctoral fellowship (*D* 25519) from the Hungarian Science Foundation (OTKA). We are grateful to F. Moreno-Insertis for helpful discussions.

## References

- Acheson D.J., 1979, *Solar Phys.* 62, 23  
 Caligari P., Moreno-Insertis F., Schüssler M., 1995, *ApJ* 441, 886  
 Caligari P., Schüssler M., Moreno-Insertis F., 1998, *ApJ* 502, 481  
 Charbonneau P., Christensen-Dalsgaard J., Henning R., et al., 1999, *ApJ* 527, 445  
 Choudhuri A.R., Gilman P.A., 1987, *ApJ* 316, 788  
 Choudhuri A.R., Schüssler M., Dikpati M., 1995, *A&A* 303, 29  
 D'Silva S., Choudhuri A.R., 1993, *A&A* 272, 621  
 Durney B.R., 1995, *Solar Phys.* 160, 213  
 Fan Y., Fisher G.H., DeLuca E.E., 1993, *ApJ* 405, 390  
 Gilman P.A., Fox P.A., 1997, *ApJ* 484, 439  
 Howe R., Christensen-Dalsgaard J., Hill F., et al., 2000, *Sci* 287, 2456  
 Hughes D.W., 1985, *Geophys. Astrophys. Fluid Dynamics* 32, 273  
 Hughes D.W., Cattaneo F., 1987, *Geophys. Astrophys. Fluid Dynamics* 39, 65  
 Leighton R.B., 1969, *ApJ* 156, 1

- MacGregor K.B., Charbonneau P., 1997, ApJ 486, 484  
Moreno-Insertis F., Schüssler M., Ferriz-Mas A., 1992, A&A 264, 686  
Parker E.N., 1987a, ApJ 312, 868  
Parker E.N., 1987b, ApJ 321, 984  
Parker E.N., 1987c, ApJ 321, 1009  
Parker E.N., 1993, ApJ 408, 707  
Rüdiger G., von Rekowski B., Donahue R.A., Baliunas S.L., 1998, ApJ 494, 691  
Schüssler M., Caligari P., Ferriz-Mas A., Moreno-Insertis F., 1994, A&A 281, 69  
Spiegel E.A., Zahn J.-P., 1992, A&A 265, 106  
Tobias S.M., Brummell N.H., Clune T.L., Toomre J., 1998, ApJ 502, 177  
Tóth G., 1996, Astrophys. Lett. & Comm. 34, 245  
Wang Y.-M., Sheeley N.R. Jr, 1991, ApJ 375, 761